Depth and geoid anomalies over oceanic hotspot swells: A global survey

Marc Monnereau, Anny Cazenave

JOURNAL OF GEOPHYSICAL RESEARCH, VOL. 95, NO. B10, PAGES 15,429–15,438, SEPTEMBER 10, 1990

DEPTH AND GEOID ANOMALIES OVER OCEANIC HOTSPOT SWELLS : A GLOBAL SURVEY

Marc Monnereau and Anny Cazenave

Centre National d'Etudes Spatiales, Groupe de Recherche de Géodésie Spatiale, Toulouse, France

Abstract. The broad depth and geoid anomalies associated with 23 hotspot swells in oceanic areas have been analyzed. Maximum height and geographical extent of the topographic swell, and of the geoid anomaly as well, have been measured for each hotspot. The results indicate a clear increase of the topographic swell height with age of the underlying lithosphere, from values in the range 300-500 m at young ages to values in the range 1500-2000 m at ages larger than 100 Ma. The geoid anomaly amplitude also increases with plate age from nearly zero close to mid-ocean ridges, to 6-8 m over old plates. On the other hand, the geographical extent of the swell does not show any clear relationship with plate age. The mean lateral extent of swells range from 1000 to 1500 km. Swells located close to spreading ridges show a significant non zero depth anomaly but are associated with negligeable geoid signal. These results complete those of a previous study where the apparent compensation depth of oceanic hots pot swells was showed to increase linearly with the square root of plate age and coincide roughly with the base of the thermal lithosphere. This trend may either be interpreted in terms of lithospheric thinning or dynamical support. Besides both seem necessary to explain the observed bathymetry, in proportion evolving with aging of the lithosphere.

1. Introduction

Classically, oceanic hotspots correspond to present or recently active volcanism producing in many instances linear seamount or island chains. Several hotspots, in particular those located far from spreading ridges, are associated with broad well-developed topographic and geoid swells of 1000-1500 km in extent.

A number of conspicious hotspot swells have been the subject of detailed geophysical analyses: the Hawaiian swell [Crough, 1978; Detrick and Crough, 1978; Detrick et al., 1981; Von Herzen et al., 1982; McNutt and Schure, 1986], the Bermuda Rise [Crough, 1978; Detrick et al., 1986], the Cape Verde Rise [Crough, 1978; Courtney and White, 1986; McNutt, 1988], the Marquesas swell [Fischer et al., 1986, McNutt et al., 1989], and the Canary Islands swell [Filmer and McNutt, 1989].

From these studies, some general conclusions have been drawn: Topographic swells are 1.-1.5 km in height. They are correlated with positive geoid anomalies of several meters amplitude. Estimates of the compensation depth of these swells give values ranging from ~50 km to ~100 km, corresponding to depths generally considered well inside the thermal plate thickness. Crough [1983] reviewed the various mechanisms able to produce hotspot swells. There is a general acceptance that swells have a thermal origin with two classes of mechanisms being regularly considered: the thermal plate thinning and the dynamical support by a convective ascending plume. While it is unanimously admitted that lithospheric thinning by thermal conduction is unable to explain the rapid rate of swell uplift observed at some hotspots, thermal erosion of the lithospheric plate by alleged small-scale convective instabilities as proposed by Yuen and Fleitout [1985] or Dalloubeix and Fleitout [1989] can be accomplished on a time scale required by the observations (<10 m.y.). Dynamical support by constant viscosity convection in the upper mantle fails to account for the shallow compensation depth of swells. On the other hand, models of convective flow crossing a sublithospheric low-viscosity channel can explain the general characteristics of the few well-documented swells [Robinson and Parsons, 1988; Ceuleneer et al., 1988].

There is not yet concensus on the best working process. This results from the fact that both mechanisms (plate thinning and convective models) are alternately put forward to explain surface observables: the Hawaiian and Marquesas swells, for example, are compatible with the plate thinning model [Detrick and Crough, 1978], whereas the same model cannot explain the Cape Verde swell, for which a contribution of convective origin is invoked [Courtney and White, 1986; McNutt, 1988].

The two classes of models have been essentially developed to explain the characterics of the well-documented swells quoted above. All of them lie on old seafloor. Hotspot swells lying over young seafloor or nearby a ridge crest have been much less studied. It is nevertheless recognized that, except for Iceland, they are smaller in height. Crough [1983] made a clear distinction between ridge crest swells and midplate swells. He proposed different processes to explain ridge crest swells on one hand and midplate swells on the other hand; the former resulting from anomalously low-density asthenospheric material, the latter from thermal plate thinning. In fact, it is more and more clear that there are not two categories of swells and that specific hotspot swells such as the Hawaiian or Bermuda swell cannot be considered as representing the norm. Rather, swells present evolving properties depending on the age of the crust they lie on. Menard and McNutt [1982] first showed that the depth of swell summits varies with age of crust. Their analysis suggested that crust younger than 10 Ma is reelevated to depths comparable to a ridge crest, while

Paper number 89JB-03784.
0148-0227/90/89JB-03784$05.00

older seafloor (10-90 Ma) is reelevated to about one third of the amount it had subsided since the ridge axis.

More recently, we considered a large number of oceanic hotspots and determined the depth of compensation of the topographic swell by analysing simultaneously geoid and topography data over the swell area [Monnereau and Cazenave, 1988; Hereafter referred to as paper 1]. We showed that the compensation depth of oceanic swells presents a linear dependence with the square root of plate age t, of the form 7. $t^{1/2}$ (km m.y.$^{-1/2}$), and corresponds to ~70% of the thermal (half-space cooling) plate thickness. In the present study, we complete the analysis conducted in paper 1 and determine over the same set of hotspots the amplitude and geographical extent of the topography and geoid anomaly. We show that as for the compensation depth, topographic height and geoid anomaly amplitude increase with age of plate while swell extent appears independent on age. In addition, we show that hotspots located over young seafloor are associated with nonnegligible topographic swell height, even very close to the ridge crest. These new trends have to be accounted for in any model proposed for hotspot swells. The evidence for evolving properties with age suggest that thermal cooling of the lithosphere exerts an influence on the mechanism responsible for the swell and favors a single process for the origin of these features.

2. Data

The data analyzed in this study are essentially the same as those used in paper 1. Twenty-three oceanic swells distributed into the three main oceans have been considered. These include Ascension, Azores, Bermuda, Bouvet, Great Meteor, Fernando, Canary, Cape Verde, St. Helena, Madeira, Rio Grande, Tristan in the Atlantic ocean, Crozet, St. Paul-Amsterdam, and Reunion in the Indian Ocean and Easter, Galapagos, Hawaii, Marquesas, Pitcairn, Samoa, Society, and Tubuaii in the Pacific ocean. These represent nearly the majority of oceanic hotspots (except for Iceland and Kerguelen) and correspond to a great diversity in lithospheric age. For example, Easter, Bouvet, St. Paul-Amsterdam and Galapagos lie over very young plate (less than 10 Ma) while Bermuda, Canary, Madeira, and Cape Verde are located on seafloor older than 100 Ma.

Initial bathymetry data from the DBDB5 file at 5 arc min interval have been averaged on a 0.5° x 0.5° grid. Thermal subsidence and sediment loading have been removed from the DBDB5 averaged bathymetry data to produce depth anomalies. Seafloor ages, interpolated on a 0.5° x 0.5° grid are based on the Larson et al. [1985] isochron map. The details for the thermal subsidence and sediment thickness corrections are given by Cazenave et al. [1988] and paper 1.

Geoid height data from Marsh et al. [1986] have been corrected from the long wavelength signal (>4000 km) due to deep mantle processes by removal of a low degree and order (up to 10) reference geopotential [Reigber et al., 1985]. The residual geoid has then been corrected for lithospheric cooling effects (see also Cazenave et al. [1988] and paper 1 for the details of these corrections). The geoid and depth anomaly maps in level contour over the 23 hotspot swells are presented in paper 1. They are not reproduced here.

3. Analysis and Results

The purpose of this analysis is to estimate the amplitude and average extent of the topographic swell and of the associated geoid anomaly.

Using the corrected depth and geoid data gridded at 0.5° interval, we have interpolated radial profiles 1000 km long originating at the center of the swell. The center of the swell is defined by the main volcanic edifice that tops it.

Sixteen radial profiles, regularly spaced, cut the swell. Cutting of the swell by assuming radial symmetry is acceptable for many swells. But clearly, radial symmetry assumption does not work for some of them, in particular

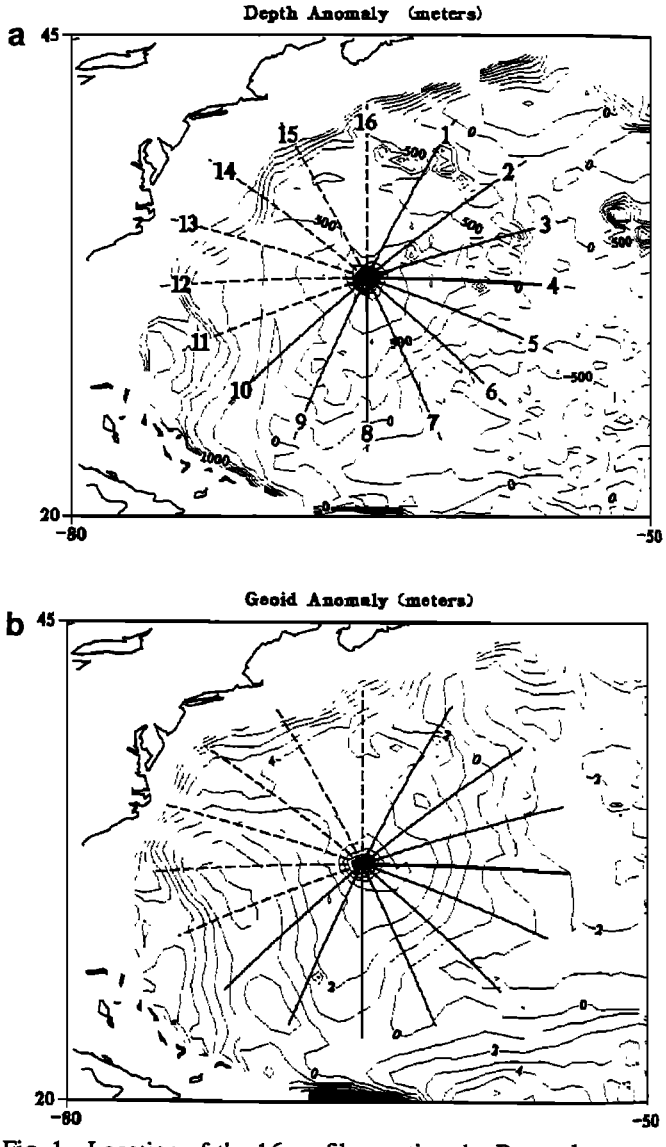

Fig. 1. Location of the 16 profiles cutting the Bermuda swell. (a) depth anomaly map. (b) geoid anomaly map. Dashed lines correspond to profiles crossing the continental margin. These are not used to estimate the topography and geoid anomaly.

for the Hawaiian swell because of its well-known elongated shape. For this swell, we excluded profiles within 30x apart from the island chain direction. In some cases, we have excluded profiles crossing geological features unrelated to the swell, for example, the continental margin east of Cape Verde, Madeira and Canary, the subduction zone west of Samoa and fracture zones for some other swells. Figure 1 shows cutting of the depth and geoid swell over Bermuda by the 16 regularly spaced profiles. Figure 2 shows the 16 topography and geoid profiles respectively over the Bermuda swell.

We have estimated the swell amplitude and extent along each of the radial profiles and along an average profile obtained by stacking the 16 profiles. We have estimated the amplitude and width of the topography and geoid anomaly by fitting the observed profiles by a Gaussian function (see Figure 2). To avoid contamination from the volcanic edifice in the topography and from its isostatic compensation by lithospheric flexure in the geoid, we have omitted data in the vicinity of the central seamount. The amount of data omitted has been chosen by eye. Depending on each case, data within 200-500 km from center of the swell have been excluded. Figure 3 shows the average topography and geoid profiles over the 23 hotspot swells considered in this study. The profiles are arranged by increasing seafloor age. Amplitudes (in the geoid and in the topography) and average swell extent are gathered in Table 1. Two amplitude estimates are reported in Table 1: the mean value of the ind ividual profiles estimates and the estimate for the average profile. In the following, we consider only the former value. The standard deviation associated with the amplitude estimate is based on the dispersion in the amplitude estimates on individual profiles. The standard deviation expresses mainly the departure from axial symmetry assumed for the shape of the swell. Geophysical signal unrelated to the swell also contributes to the reported standard deviation.

Height of Swell

Swell height estimates range from ~300-500 m to values larger than 2 km. Several hotspots are located near a ridge crest, such as Ascension, Amsterdam, Easter, and Galapagos (seafloor age less than 10 Ma). The associated swell height is low but appears significantly above the noise level. It ranges from 300 ± 100 m at St. Paul-

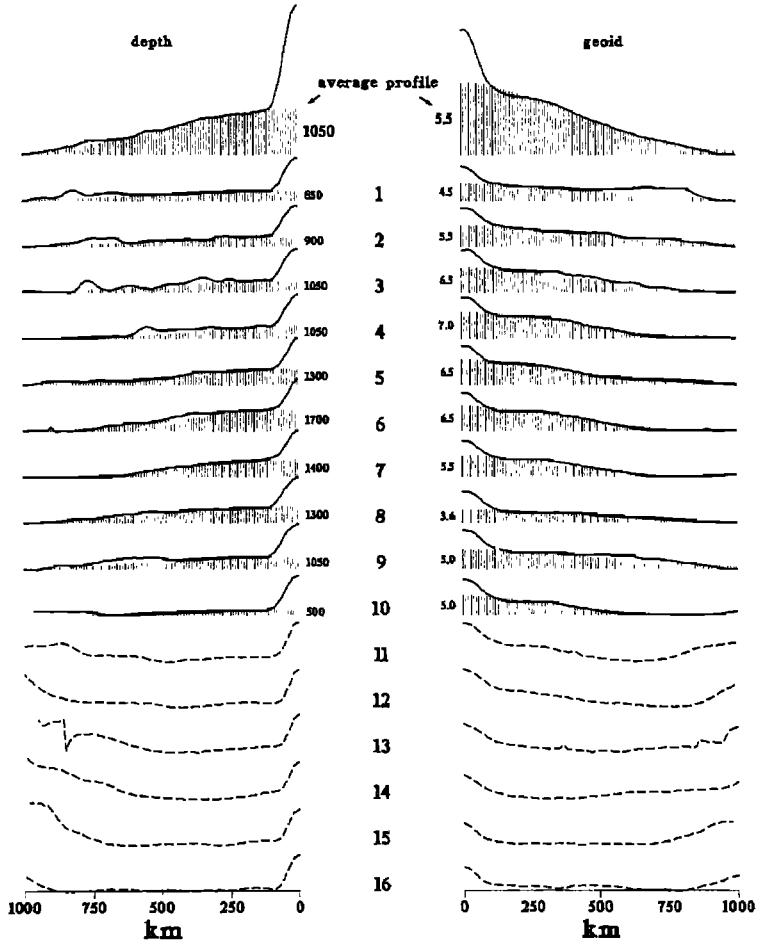

Fig. 2. Topography and geoid anomaly in profile form from the center of the Bermuda swell along the 16 tracks numbered as in Figure 1. The right and left upper curves represent the average profile using the individual tracks. Solid and dashed lines are observed profiles. Hatched areas represent the best fitting Gaussian function.

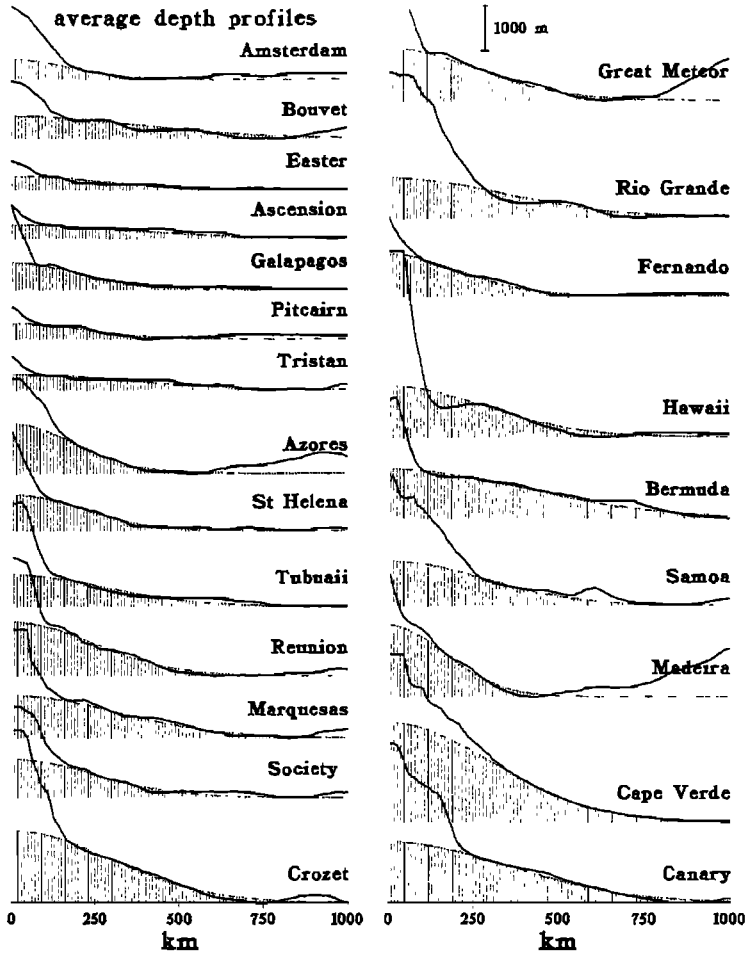

Fig. 3a. Topography anomaly in profile form (average profile) for each of the 23 hotspot swells considered in this study.

Amsterdam, the swell the closest to a ridge crest (seafloor age < 2 Ma) to 600 ± 100 m at Galapagos (seafloor age of 9 Ma). The Easter swell height (age of 3 Ma) is also small but significant (350 ± 150 m), a value comparable to that observed at St. Paul-Amsterdam. Several swell heights rise above the 1 km level (e.g., Azores, Bermuda, Cape Verde, Madeira, Canary, Crozet, Reunion, Hawaii, and Samoa). Except for Azores, they all lie on seafloor older than 50 Ma. In fact, we observe a clear progressive increase of swell height with seafloor age. In Figure 4, swell height is plotted as a function of crustal age at the hotspot location. The increasing trend is quite apparent. It confirms earlier results from Menard and Mc[Nutt [1982] based on the estimate of the depth of swell summit, i.e. without seafloor subsidence nor sediment loading corrections. In addition, our swell height estimates are in good agreement with those given in Davies [1988].

The trend observed in Figure 4 is compatible with a linear increase of swell height h with square root of age t, although a linear dependence on age could fit the data as well. A square root of age dependence is preferred, however, since it is expected in the context of the thermal evolution of the lithosphere. Since it is clear from Figure 4 that height of swells located on or near the ridge axis is nonzero, the adjusted function will not go through the origin. The best fitting relationship between h and t is

$$h = 285.\ (\pm 5.5) + 81.8\ (\pm 6.8)\ \sqrt{t} \qquad (1)$$

where h is in meters and t in Ma. Note that Azores, Crozet and Cape Verde swells lie well above the average trend.

Geoid Swell Amplitude

Examining the results reported in Table 1, we notice that the amplitude of the geoid anomaly increases with seafloor age. It varies from about zero at ridge crest swells to ~6 m on very old seafloor. This is illustrated in Figure 5 showing the amplitude of the geoid anomaly plotted as a function of age. However, contrarily to the case of the topography anomaly, swells located on young seafloor are associated with negligeable signal in the geoid. A linear increase of the geod height N with age t fits well the data. Linear regression gives

$$N = -0.05\ (\pm 0.2) + 0.041\ (\pm 0.003)\ t \qquad (2)$$

with N in meters and t in Ma. Again, Azores, Crozet, and Cape Verde have a geoid anomaly larger than the average trend.

We have measured the lateral extent of each swell using the 16 topography profiles as well as the average profile.

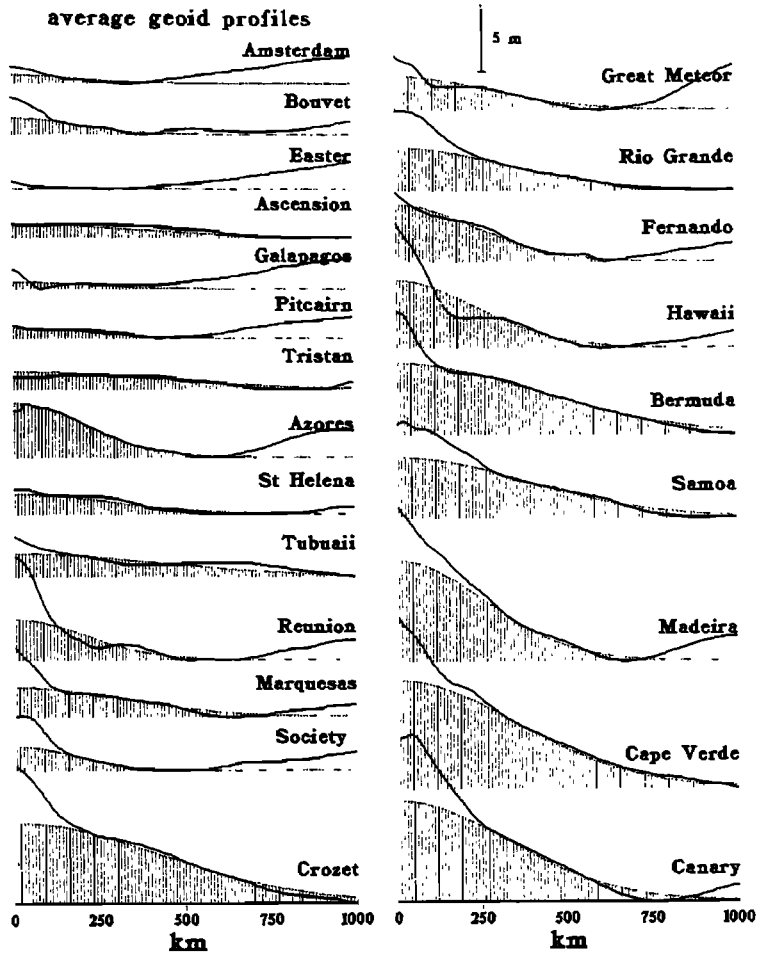

Fig. 3b. Same as Figure 3a, but for the geoid anomaly. Hatched areas represent the best fitting Gaussian function.

TABLE 1. Hotspot Swell Identification, Age of Plate, Swell Height, Geoid Anomaly Amplitude, and Swell Extent

Hotspot Swell Identification		Age of Crust at the Hotspot, Ma	Swell Height, m			Geoid Anomaly, m			Swell Extent, km	
			Mean Value a		Estimate b	Mean Value a		Estimate b		
Amsterdam	(AMS)	<2	500	±100	450	0.0	±0.5	0.6	1200	±200
Bouvet	(BOU)	<2	700	±150	500	0.0	±0.5	1.2	900	±100
Easter	(EAS)	3	350	±150	300	0.0	±0.5	0.0	1000	±200
Ascension	(ASC)	5	450	±150	300	0.40	±0.4	1.0	1500	±200
Galapagos	(GAL)	9	600	±100	600	0.40	±0.4	0.5	1200	±200
Pitcairn	(PIT)	16	400	±100	350	0.40	±0.4	0.8	1300	±100
Tristan	(TRI)	20	600	±100	350	1.00	±0.3	1.3	1000	±100
Azoes	(AZO)	32	1200	±100	1100	3.00	±1.0	4.0	1100	±100
StHelena	(STH)	37	750	±100	800	1.25	±0.3	1.5	1100	±100
Tubuai	(TUB)	44	650	±150	700	1.80	±0.2	1.7	1000	±100
Reunion	(REU)	63	1100	±200	1200	2.60	±0.6	3.0	1000	±100
Marquesas	(MAR)	64	950	±100	950	2.25	±0.8	2.2	1300	±100
Society	(SOC)	74	750	±150	850	2.00	±0.5	1.8	900	±100
Crozet	(CRO)	76	1700	±100	1600	6.50	±1.0	6.0	1600	±100
GreatMeteor	(GTM)	85	1100	±100	1200	3.00	±0.5	2.5	1100	±100
RioGrande	(RIO)	90	950	±150	900	3.30	±0.5	3.2	1400	±200
Fernando	(FER)	99	1050	±150	950	4.50	±0.5	4.2	1000	±100
Hawaii	(HAW)	100	1200	±200	1150	5.00	±1.0	5.0	1450	±150
Bermuda	(BER)	117	1200	±100	1100	5.50	±0.5	5.3	1800	±100
Samoa	(SAM)	120	100	±100	1000	4.75	±1.3	4.5	900	±100
Madeira	(MAD)	135	1550	±150	1600	6.50	±0.7	7.5	1000	±200
CapeVerde	(CAP)	140	2100	±200	2200	8.00	±0.5	8.0	1750	±150
Canary	(CAN)	176	1500	±100	1350	6.80	±1.2	7.5	1500	±150

a Mean value of the individual profiles estimates.
b Estimated on the average profile.

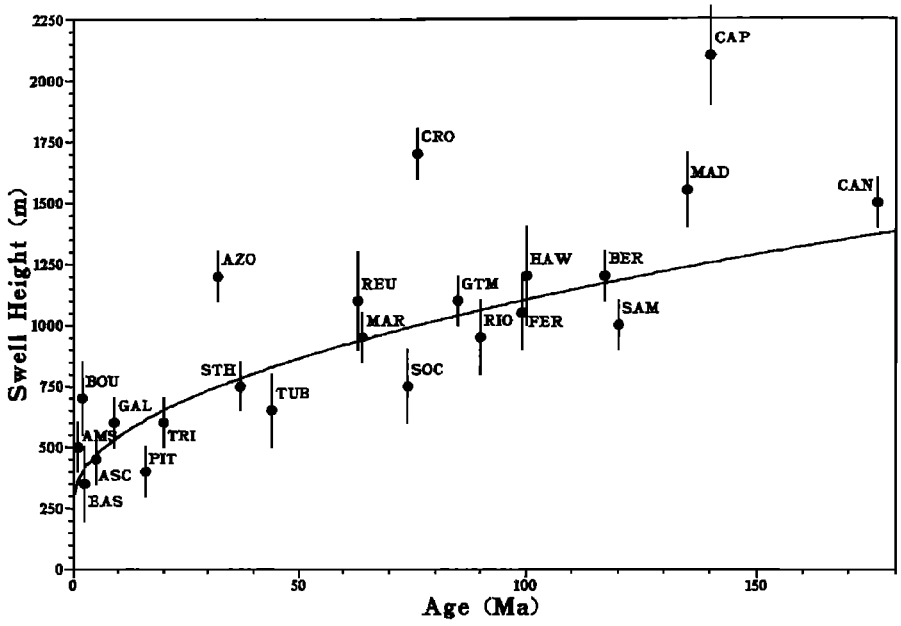

Fig. 4. Swell height estimated at the 23 hotspot as a function of age (see Table 1 for symbols). The solid line is the best fitting square root of age function.

Because swells are two-dimensional features of irregular shape, the lateral extent we measure from the profiles represents a mean value of the actual dimensions of the swell. It would correspond to the diameter of a swell having axial symmetry. As when estimating swell height and geoid anomaly, we have excluded some radial profiles perturbed by unrelated geological features (e.g. the continental margin east of Canary and Cape Verde). In the case of Hawaii, the swell extent is measured using profiles transverse to the island chain direction.

Estimates of the swell extent are reported in Table 1. All swells appear to be at least 1000 km. Bermuda, Crozet, Cape Verde, and Hawaii are the largest. We have plotted the swell extent as a function of age (Figure 6). No trend is emerging, the width of the swell appearing essentially independent on age. On the other hand, plates of similar age can support swells showing 50% variation in width: see, for example, Crozet and Society or Bermuda and Fernando. Bermuda is one of the largest swells while Fernando is one of the smallest. The narrow extent of the

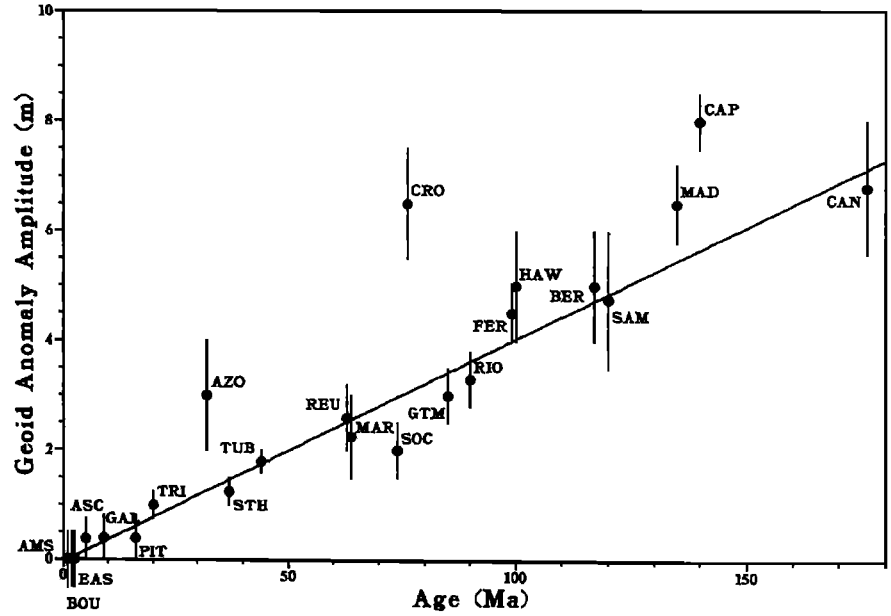

Fig. 5. Geoid anomaly amplitude estimated at the 23 hotspots as un function of age (see Table 1 for symbols). The solid line is the best fitting regression line.

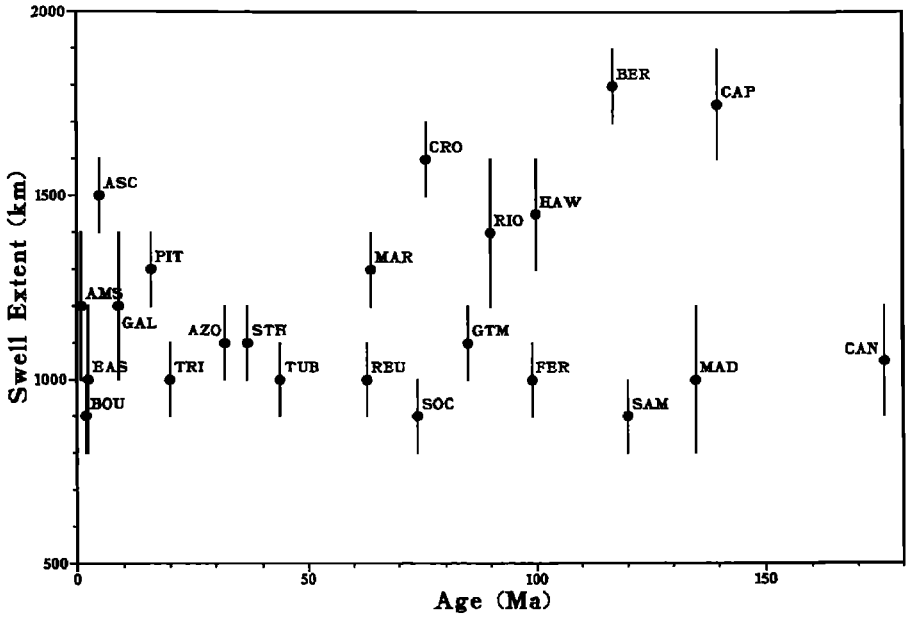

Fig. 6. Spatial extent swells as a function of age (see Table 1 for symbols).

Fernando swell could be because of the proximity of the continental margin.

4. Discussion

According to the results presented above, the medium wavelength (~2000 km) topography and geoid anomalies associated with oceanic hotspots evolve with age of plate with a rather progressive behavior. Hotspots located close to a ridge crest present a significantly nonzero topographic swell of ~300 m amplitude. The corresponding geoid signal, however, is negligeable. To first order, swell height increases linearly with the square root of plate age whereas geoid anomaly amplitude increases linearly with age.

The swell topography h increases of ~800 m in 100 m.y. while the geoid height N increases of ~4 m in the same age range. The reported dependence of h and N on age indicates that the geoid to depth ratio N/h increases with the square root of age, with N/h proportional to 0.5 t1/2. This rate of change of N/h is exactly the value obtained in paper 1 from a two-dimensional estimate of the slope between geoid and depth over individual hotspots (see Figure 7). The perfect agreement obtained between these independent determinations of the variation with age of the geoid to depth ratio gives some confidence in the individual relationships reported here for h and N with age.

In paper 1 we deduced the apparent depth of compensation d_c of hot spot swells from this geoid to depth ratio estimate, assuming Pratt isostasy:

$$\frac{N}{h} = \frac{\pi G}{g} d_c(\rho_m - \rho_w) \quad (3)$$

ρ_m and ρ_w are mantle and seawater densities, G is the gravitational constant, and g is the mean surface gravity.

According to relations (1) and (2), we have also

$$\frac{N}{h} = 0.5\sqrt{t} - 0.7 \quad (4)$$

Then assuming $\rho_m = 3300$ kg m^{-3}, and $\rho_w = 1000$ kg m^{-3}, it becomes

$$d_c = 10.\sqrt{t} - 14. \quad (5)$$

with d_c in kilometers and t in Ma. This value corresponds roughly to the thermal plate thickness. In paper 1, we proposed $d_c = 7.\sqrt{t}$ as the best fitting relationship where we imposed $d_c = 0$ at t= 0 for consistency with the assumption of purely lithospheric default mass.

For a given value of the geoid to depth ratio, we may find a different d_c value if we assume Airy type isostasy. Sandwell and McKenzie (1989) have developped such a model, the "thermal swell model", where the swell topography is compensated by low density material intruded in the eroded lithosphere. In this case, the average depth of compensation is related to N/h through

$$\frac{N}{h} = 2\frac{\pi G}{g}[d_c(\rho_m - \rho_c) - d_w(\rho_c - \rho_w) - d_m(\rho_m - \rho_c)] \quad (6)$$

where ρ_c is crust density and d_w and d_m are seafloor depth and Moho depth respectively. This relation takes into account the deflection of the moho and the crust. It is important to notice that these deflexions produce negative N/h near the ridges as reported in paper 1. Assuming $d_w = 4$ km, $d_m = 11$ km, and $\rho_c = 2800$ kg m^{-3}, it becomes

$$\frac{N}{h} = 0.094\, d_c - 0.49 \quad (7)$$

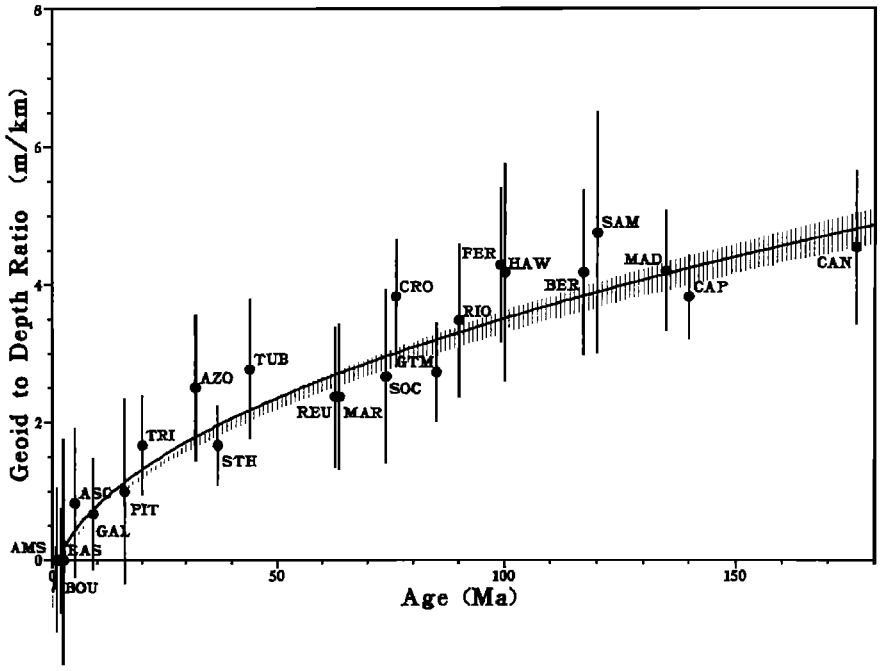

Fig. 7. Geoid to depth ratio as a function of age and computed from the swell height and geoid anomaly estimated in this study. The solid line is the best fitting square root of age function. Hatched area correspond to the values estimated by Monnereau and Cazenave [1988]. (see Table 1 for symbols.)

In this case, the average depth of compensation is exactly one half of the previous one. This is not a contradiction between the two models. This reflects the different meaning of d_c in the Pratt and "thermal swell" models. In the former, d_c is the depth below which lateral density contrast no more exists and in the latter d_c corresponds to the depth of the barycenter of the default mass. Thus the Pratt or Airy mechanisms both suggest that compensation of hot spot swells is entirely lithospheric. Besides, one should note that according to the "thermal swell" model, when the lithosphere is entirely eroded, seafloor and geoid anomalies rise up to values of mid-ocean ridges, i.e., swell height equals subsidence and geoid anomaly equals geoid slope undergone prior to the reheating event.

In the half space cooling model, the expression of the geoid slope N to the subsidence w ratio is [Turcotte and Schubert, 1982]

$$\frac{N}{w} = \frac{\pi G}{g} (\rho_m - \rho_w) \left[1 + \frac{2 \rho_m \alpha T_m}{\pi (\rho_m - \rho_w)} \right] \sqrt{\pi \kappa t} \qquad (8)$$

where κ is the thermal diffusivity, α the thermal expansion coefficient and T_m the mean asthenospheric temperature ($\kappa = 8.\ 10^{-7}\ m^2\ s^{-1}$, $\alpha = 3.5\ 10^{-5} °C^{-1}$, $T_m = 1350°C$). Then $N/w = 0.5 \sqrt{t}$. This value is similar to that found for N/h for swells. Hence the N/h ratio does not constrain the amount of thinning and does not appear as specific to hot spot swells. Now, althought the reported N/h ratio is fully rendered by the "thermal swell" model, so does a dynamical point of view.

Indeed, Parsons and Daly [1983] and Robinson and Parsons [1988] have shown that shallow compensation depths within the lithosphere can be produced by convective circulations underlaying that lithosphere. Ceuleneer et al. [1988] showed that the square root of age increase of the geoid to depth ratio reported in paper 1 could be satisfactorily explained by a mantle convective plume under the hotspot crossing a sublithospheric low-viscosity layer whose bottom remains at a fixed depth (~200 km) and whose thickness decreases at the expense of the thermally thickening lithospheric plate. A viscosity of ~2.5 10^{19} Pa s was proposed for the low-viscosity layer as best fitting model predictions and data. These convective calculations take into account the interaction of the ascending flow with the low-viscosity layer but ignore the thermal interaction with the lithosphere. Thus the predicted behavior of swell height and geoid anomaly with age corresponds to the dynamical contribution only. Although the geoid to depth ratio is well predicted, the increase in swell topography with the age of the lithosphere is too low by a factor ~2 compared to what is observed. This clearly indicates that a lithospheric contribution (thermal erosion of the lithosphere) has to be invoked to account for the observed swell topography.

Conversely, the swell topography associated with hotspots at mid-ocean ridges seems to imply a dynamical support. Let us consider the ratio between height h and seafloor subsidence w (referred to the ridge axis) as predicted by the half-space cooling model [e.g. Turcotte and Schubert, 1982]. In Figure 8, we have plotted the h/w ratio as a function of age. If we except swells located on very young seafloor (Amsterdam, Easter, and Bouvet), the h/w ratio is roughly constant with age, of the order of 0.3. This result agrees perfectly with that of Menard and McNutt [1982] stating that at hotspot locations, seafloor

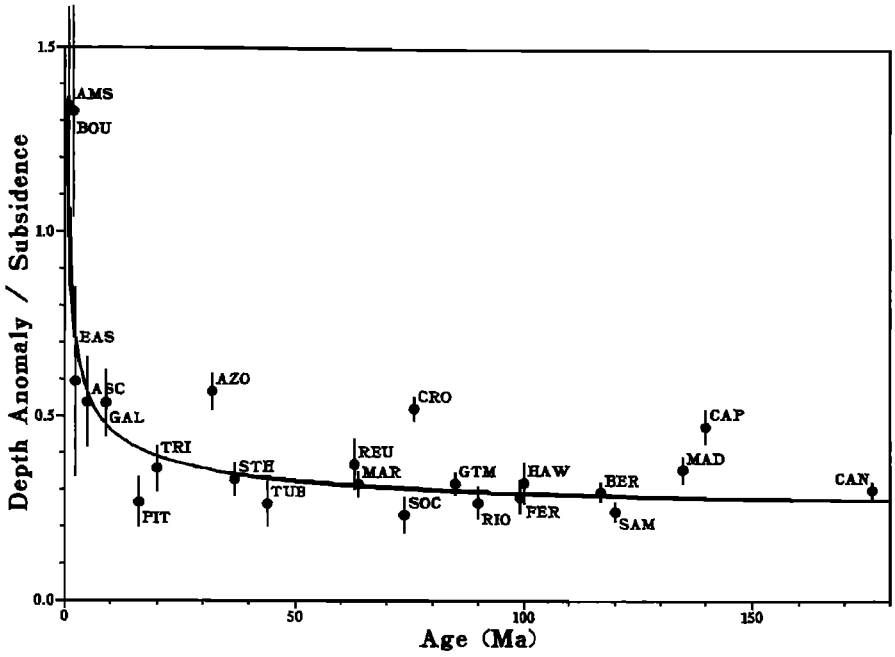

Fig. 8 : Swell height to subsidence ratio as a function of age. (See Table 1 for symbols).

depth is reelevated to ~1/3 of the subsidence amount. Menard and McNutt indicated moreover that young seafloor swells are reelevated to depths comparable to ridge crest depth. Our analysis does not contradict the latter point. It shows that the depth of the swell summit may lie below or above the mean reference ridge crest depth (from which the subsidence w is estimated): Figure8 shows th at for the very young seafloor swells; the h/w ratio ranges from 0.6 to 1.35. These observations suggest in fact that the effective height of ridge crest swells contributes to the observed variable elevation of mid ocean ridges. Therefore young seafloor swells are quite likely supported dynamically, the more as the lithospheric reheating hypothesis evidently cannot be invoked in this case. According to relations (1), we can write $h = a\sqrt{t} + b$. We have also $w = c\sqrt{t}$. a, b and c are constants. Then the geoid to depth ratio can be written as $\frac{h}{w} = \frac{a}{c} + \frac{b}{c\sqrt{t}}$. Numerically, we have

$$\frac{h}{w} = 0.215 + \frac{0.74}{\sqrt{t}} \qquad (9)$$

h/w is equal to 0.29 at 100 Ma. The very good agreement between relation (9) and the whole data set (Figure 8) shows that the swells amplitude actually evolves continuously from 0 to 180 Ma. This suggests that the swell bathymetry results of both a dynamical contribution and a thermal contribution due to the aging of the lithosphere. In order to quantify the latter component we assume that a sudden thermal thinning of the base of plate induces, by isostatic balance, a lithospheric uplift. In this context, the geotherm of the thinned plate is unchanged. Below, asthenospheric material intrudes the eroded plate. The swell height minus the dynamical contribution of 300 m is accounted for this uplift. We can deduce the depth of the base of the thinned plate or equivalently, the temperature associated with this depth [see for example Von Herzen et al., 1982]. Assuming an half space geotherm and the same numerical values as above for the thermal parameters , we find that the base of the thinned plate approximately corresponds to the 900°C-1000°C isotherm. Above this isotherm, the mantle is rigid with regard to the time scale of the geodynamic processes [Darot and Guegen, 1981]. So, the thinning of the lithosphere could be a mechanical erosion of the most ductile part of the lithosphere by a mantle plume.

In Figure 4, 5, and 8, swell height and geoid anomaly of Azores, Crozet and Cape Verde lie above the mean trends. This could evidence for an important perturbation of the lithospheric geotherm. These swells are located on motionless plates with respect to the hot spot reference frame. Thus one would expect that an ascending plume would have sufficient time to reheat the lithosphere which would result in extremal uplifts and geoid anomalies.

5. Conclusion

Owing to the agreement between the result of this study and those of paper 1, where the data were processed using independent methods, the variations with age of hotspot swell properties (geoid anomaly, bathymetric uplift, and their ratio) are well established. We believe that it is not unreasonable to invoke a single mechanism (convective flow) to explain all oceanic hotspot swells; this mechanism inducing possibly evolving effects in proportion as it develops from young lithosphere to old lithosphere.

Clearly, only convective calculations with variable rheology in order to take account of the interaction of the flow not only with the low-viscosity layer but also with the lithosphere will shed some light on the respective contributions of dynamical origin on one hand, of lithospheric origin on the other hand wich produce the observed characteristics of hotspot swells.

Acknowledgments: We would like to thank D.Sandwell, B.Marsh and an anonymous reviewer for their comments. We thank also S. Calmant and G. Ceuleneer for helpful discussions. Contibution INSU-CNRS-DBT n°165, Thème Dynamique Globale.

References

Cazenave, A., K. Dominh, M. Rabinowicz, and G. Ceuleneer, Geoid and depth anomalies over ocean swells and throughs: Evidence for an incrasing trend of the geoid to depth ratio with age of plate, *J. Geophys. Res., 93*, 8064-8077, 1988.

Ceuleneer, G., M. Rabinowicz, M. Monnereau, A. Cazenave, and C. Rosemberg, Viscosity and thickness of the sublithospheric low viscosity zone: Constraints from geoid and depth over oceanic swells, *Earth Planet. Sci. Lett., 89*, 84-102, 1988.

Courtney, R.C., and R.S. White, Anomalous heat flow and geoid across the Cape Verde Rise: Evidence for dynamic support from a thermal plume in the mantle, *Geophys. J. R. Astron. Soc., 87*, 815-867, 1986.

Crough, S.T., Thermal origin of hot spot swells, *Geophys. J. R. Astron. Soc., 55*, 451-469, 1978.

Crough, S.T., Hot spots swells, *Annu. Rev. Earth Planet. Sci., 11*, 165-193, 1983.

Dalloubeix C., and L. Fleitout, Convective thinning of the lithosphere: A model constrained by geoid observations, *Phys. Earth Planet. Inter., 57*, 330-343, 1989.

Darot, M., and Y. Guegen, High temperature creep of forstherite single crystal, *J. Geophys. Res., 86*, 6219-6234, 1981.

Davies, G.F., Ocean bathymetry and mantle convection 1, Large scale flow and hotspots, *J. Geophys. Res., 93*, 10,467-10,480, 1988.

Detrick, R.S., and S.T. Crough, Island subsidence, hot spots, and lithosphere, *J. Geophys. Res., 83*, 1236-1244, 1978.

Detrick, R.S., R.P. Von Herzen, S.T. Crough, D. Epp, and U. Fehn, Heat flow on the Hawaiian swell and lithospheric reheating, *Nature, 292*, 142-143, 1981.

Detrick, R.S., R.P. Von Herzen, D. Sandwell, and M. Dougherty, Heat flow observations on the Bermuda rise an thermal models of midplate swells, *J. Geophys. Res., 91*, 3701-3723, 1986.

Filmer P.E. and McNutt M.K., Geoid anomalies over the Canary Islands group, *Marine Geophys. Res., 11*, 77-89, 1989.

Fischer, K.M., M.K. McNutt, and L. Shure, Thermal and mechanical constraints on the lithosphere beneath the Marquesas swell, *Nature, 322*, 733-736, 1986.

Marsh, J.G., A.C. Brenner, B.C. Beckley, and T.V. Martin, Global mean sea surface based upon the Seasat altimeter data, *J. Geophys. Res., 91*, 3501-3506, 1986.

McNutt, M.K., Thermal and mechanical properties of the Cape Verde Rise, *J. Geophys. Res., 93*, 2784-2795, 1988.

McNutt, M.K., and L. Shure, Estimating the compensation depth of the Hawaiian swell with linear filters, *J. Geophys. Res., 91, 13,915-13,925*, 1986.

McNutt, M.K., K. Fischer, S. Kruse, and J. Natland, the origin of the Marquesas fracture zone ridge and its implication for the nature of hotspots, *Earth Planet. Sci. Lett., 91*, 381-394, 1989.

Menard, H.W. and, M.K. McNutt, Evidence for and consequences of thermal rejuvenation, *J. Geophys. Res., 87*, 8570-8580, 1982.

Monnereau, M., and A. Cazenave, Variation of the apparent compensation depth of hotspot swells with age of plate, *Earth Planet. Sci. Lett., 91*, 179-197, 1988.

Parsons, B., and S. Daly, The relationship between surface topography, gravity anomalies and Temperature structure of convection, *J. Geophys. Res., 88*, 1129-1144, 1983.

Parsons, B., and J.G. Sclater, An analysis of the variation of ocean floor bathymetry and heat flow with age, *J. Geophys. Res., 82*, 803-827, 1977.

Reigber, C., G. Balmino, H. Muller,, W. Bosch, and B. Moynot, GRIM gravity model improvement using Lageos (GRIM3L1), *J. Geophys. Res., 90*, 9285-9301, 1985.

Robinson, E.M., and B. Parsons, Effects of a shallow low-viscosity zone on the formation of mid-plate swells, *J. Geophys. Res., 93*, 3144-3157, 1988.

Sandwell, D.T. and K.R. McKenzie, Geoid height versus topography for oceanic plateaus and swells, *J. Geophys. Res., 94*, 7403-7418, 1989.

Turcotte, D.L., and G. Schubert, *Applications of Continuum Physics to Geological Problems, Geodynamics*, John Wiley, New York, 1982.

Von Herzen, R.P., R.S. Detrick, S.T. Crough, D. Epp, and V. Fehn, Thermal origin of the Hawaiian swell : Heat flow evidence and thermal models, *J. Geophys. Res., 87*, 6711-6723, 1982.

Yuen, D. A., and L. Fleitout, Thinning of the lithosphere by small scale convective destabilisation, *Nature, 313*, 125-128, 1985.

A. Cazenave and M. Monnereau, Groupe de Recherche en Géodésie Spatiale, Observatoire Midi-Pyrénées, 14 avenue E. Belin, 31400 Toulouse, France.

(Received May 4, 1989;
revised July 20, 1989;
accepted December 13, 1989.)